Annals of Biomedical Engineering, Vol. 27, pp. 326–339, 1999
Printed in the USA. All rights reserved.

Theoretical Gas Phase Mass Transfer Coefficients for Endogenous Gases in the Lungs

PETER CONDORELLI and STEVEN C. GEORGE

Department of Chemical and Biochemical Engineering and Materials Science, University of California at Irvine, Irvine, CA

(Received 18 November 1997; accepted 9 February 1999)

Abstract—Gas phase mass transfer coefficients for nitric oxide (NO), ethanol (EtOH), and water vapor (H_2O) were determined for typical conducting airway geometry and tracheal flows (5×10^{-5} and $5\times10^{-4}\ m^3\ s^{-1}$), by solving the steady-state two-dimensional diffusion equation. A constant absolute production rate with first order consumption reactions in pulmonary tissue was assumed for NO. For EtOH and H_2O, constant concentrations were assumed in the blood and tissue, respectively. Results, expressed in terms of the average Sherwood number ($\overline{Sh}$), were correlated with the Peclet (Pe_r) number, and the length-to-diameter (L/D) ratio for each airway branch in terms of a lumped variable, $Pe_r(L/D)^n$. ($\overline{Sh}$) increases as the solubility of the gas in tissue and blood increases. In addition, $\overline{Sh}$ passes through a minimum value at $Pe_r(D/L)^n$ equal to approximately one when axial convection and diffusion have equal but opposite magnitudes. We conclude that $\overline{Sh}$ is not a monotonic function of $Pe_r(L/D)^n$ within the entire airway tree and that it depends on the physical properties of the gas in the tissue. This conclusion contrasts with previous experimental and theoretical correlations. © *1999 Biomedical Engineering Society.* [S0090-6964(99)01403-4]

Keywords—Bifurcation, Tubes, Airways, Diffusion, Sherwood number, Pulmonary.

INTRODUCTION

The detection of compounds in the exhaled breath has important medical and legal applications. Nitric oxide (NO), a reactive but sparingly soluble gas, is produced within the tissue of the airways of the lungs.[16] As an intercellular messenger, NO is involved in the modulation of blood flow, platelet inhibition, neurotransmission, the regulation of smooth muscle tone, and host defense.[7,16,26] Inhaled, exogenous NO may be an effective treatment of diseases, such as asthma, pulmonary hypertension, and adult respiratory distress syndrome.[7,26] Exhaled NO levels have recently been correlated with inflammatory diseases such as bronchial asthma.[7] Unfortunately, only limited information is available regarding the basic gas exchange dynamics of NO in the lungs.

Ingested ethanol (EtOH) is transported from the blood, through the surrounding tissue into the airway lumen,[8] and therefore may be modeled as an endogenously produced gas in the pulmonary airways. Ethanol is unreactive at low concentrations and roughly 50,000 times more soluble in tissue than NO. The concentration of EtOH in exhaled breath is often used to estimate blood alcohol concentration, however the accuracy of this technique is controversial because the interaction of EtOH with the conducting airways is only partially characterized.[8]

Water is a ubiquitous molecule in the lungs. Dry ambient air is humidified by transport of water vapor from the thin mucous membrane lining the pulmonary airways. In addition, the transfer of water (and heat) plays an important role in exercise-induced asthma.[7] For all three of these compounds, a complete model of the gas exchange dynamics requires description of the interphase transport between the airway wall and lumen. Because the lower conducting airways (bronchioles) and alveoli are essentially inaccessible to direct experimental measurement, mathematical modeling provides an avenue of understanding the gas exchange mechanisms of endogenous gases within the lungs.

Relatively detailed models simulating the pulmonary gas exchange mechanism for EtOH have been developed previously. George *et al.*[10] described the simultaneous exchange of heat, water, and a highly water soluble gas using a symmetric bifurcating structure through 18 generations for the conducting airways with the respiratory bronchioles and alveoli lumped together into a single unit. Bui *et al.*[3] extended this model by including specific radial compartments for the epithelium and smooth muscle as well as a dynamical description of the bronchial circulation. Important is that Bui *et al.*'s[3] sensitivity analysis identified the gas phase mass transfer coefficient, k_c, as a critical parameter in determining the shape of the exhalation profile. Both of these models estimated heat and mass transfer coefficients from em-

Address correspondence to Steven C. George, MD, PhD, Department of Chemical and Biochemical Engineering and Materials Science, 916 Engineering Tower, University of California at Irvine, Irvine, CA 92697-2575. Electronic mail: scgeorge@eng.uci.edu

pirical correlations developed by Ingenito *et al.*[14] and by Hanna *et al.*,[13] which predict the mass transfer coefficient to be proportional to $(\mathrm{Re})^n$, where Re is the Reynolds number of the flowing gas and ''n'' is a positive exponent $(0<n<1)$. This leads to artifacts in the lower airways, where Re becomes very small, because $k_c \rightarrow 0$ as $\mathrm{Re} \rightarrow 0$. Available literature[10,11] indicates that as $\mathrm{Re} \rightarrow 0$, $k_c \rightarrow 6\mathcal{D}/D$, where $\mathcal{D}$ is the gas phase diffusivity and D is the diameter of the airway branch.

The goal of our current study is to develop a two-dimensional (radial and axial) theoretical model that can be used to determine the gas phase mass transfer coefficient in human conducting airways. The model explores the above asymptotic relationship, and correlates the model results for use in more detailed gas exchange models.

MODEL DEVELOPMENT

Airway Geometry

The human pulmonary airways may be differentiated into two regions: the ''conducting airways,'' including the trachea, bronchi, and nonrespiratory bronchioles, and the ''respiratory airways,'' which consist of the respiratory bronchioles and alveoli. Since local heat and mass transfer coefficients in the upper respiratory tract, including the trachea, have been extensively characterized by Hanna and Scherer,[12,13] only generations 1 and beyond are considered in this study. Even though breathing is time dependent, the Womersley parameter (the ratio of the time required for propagation of viscous forces to the time to complete one breath) is small at lung conditions pertinent to tidal breathing. Thus, steady-state concentration profiles are established rapidly, and the assumption of quasisteady state is justified.[11] Inspiratory temperatures predicted by Hanna and Scherer[13] justify the approximation of isothermal conditions (37 °C). The gas phase mass transfer coefficients determined in this study are valid only in the conducting airways. The conducting airways consist of a tree-like sequence of branching tubes, which usually bifurcate by dichotomy. Hence, starting with the trachea (generation 0) each parent tube divides into two daughter tubes. Weibel[25] made extensive measurements of conducting airway geometry, and proposed a model of ''regular dichotomy,'' which described this geometry as a simplified symmetric bifurcation pattern. This model, illustrated in two dimensions by the schematic shown in Fig. 1, is used to specify the conducting airway geometry for this work. The conducting airways are defined as generations 1–17.

Each branch of the conducting airways is modeled as a constant cross-sectional tube of diameter, D (radius, R) and length, L, exhibiting bulk flow in the axial direction only (see Fig. 2). The cylindrical gas space (lumen) is surrounded by a thin annular mucous layer which is in turn surrounded by cellular tissue perfused by a network of capillaries. The gas phase concentration of the diffusing species at each branch inlet $(z=0)$ is assumed to be constant (C_0 in Fig. 2). This is justified based on the axial and radial mixing arising from secondary flows established at the bifurcations between branches.

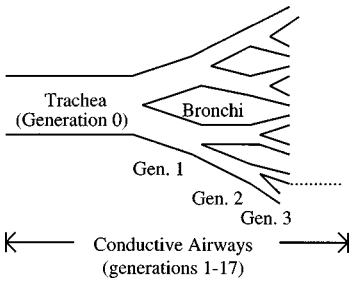

FIGURE 1. Two-dimensional representation of Weibel's (Ref. 25) regular dichotomy model for the conducting airways.

Weibel's regular dichotomy model[25] is used to specify the radius, R, and length, L, of each airway branch. The tissue layer thickness, l_t, is adjusted relative to the diameter of the specific airway with an uncertainty of roughly 20% based on the guidelines provided by Gastineau *et al.*[6] Table 1 summarizes the values of D, L, and l_t as a function of the airway generation number used in this study. The mucous layer is assumed to be a continuous sheet of uniform thickness: $l_m = 1 \times 10^{-5}$ m (10 μm) in all airways (uncertainty approximately 20%), which is consistent with the value used in previous studies.[3,9,10] Since both l_t and l_m are small compared to D, a thin film approximation is valid in the tissue and mucous layers and the effects of curvature are negligible. Thus, these regions can be modeled using rectangular coordinates.

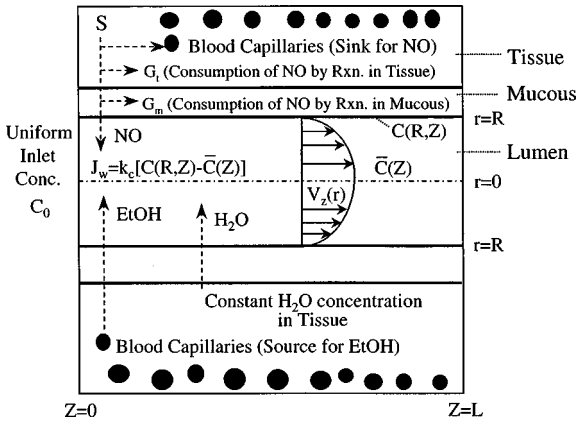

FIGURE 2. Cross-sectional view of a single branch of the conducting airways indicating key features of model development such as the source of gases, velocity profile, and definition of the mass transfer coefficient.

TABLE 1. Conducting airway geometry as a function of generation number (from Ref. 25).

Generation	D (cm)	L (cm)	l_t (μm)	L/D	l_t/D
1	1.22	4.76	100	3.9	0.008
2	0.84	1.9	72.8	2.3	0.009
3	0.56	0.76	54.0	5.4	0.01
4	0.46	1.27	46.4	2.8	0.01
5	0.36	1.07	39.4	3.1	0.012
6	0.28	0.90	34.5	3.2	0.013
7	0.24	0.76	31.0	3.3	0.014
8	0.186	0.64	28.2	3.5	0.015
9	0.154	0.54	25.4	3.5	0.017
10	0.13	0.46	24.1	3.6	0.018
11	0.11	0.39	22.8	3.6	0.021
12	0.096	0.33	21.6	3.5	0.023
13	0.082	0.27	20.7	3.3	0.025
14	0.074	0.23	20.2	3.1	0.028
15	0.066	0.20	19.6	3.1	0.030
16	0.060	0.17	19.2	2.8	0.032
17	0.054	0.14	18.7	2.6	0.035

Mass Transfer Coefficient: Definition

The mass transfer rate of an endogenously produced gas to the airway lumen from surrounding tissue in the conducting airways can be described by the gas phase mass transfer coefficient, k_c. As shown in Fig. 2, k_c is defined in terms of the diffusive flux at the wall, J_w:

$$J_w = \mathcal{D}\left.\frac{\partial C}{\partial r}\right|_{(R,z)} = k_c(C(R,z) - \overline{C}(z)), \tag{1}$$

where $\mathcal{D}$ is the gas phase diffusivity, $C(R,z)$ is the gas phase concentration at the airway wall, and $\overline{C}$ is the cross-sectional mean concentration over the lumen cross section:

$$\overline{C}(z) = \frac{2}{R^2}\int_0^R C(r,z) r\, dr. \tag{2}$$

Determination of k_c requires knowledge of the gas phase concentration distribution, $C(r,z)$.

Velocity Profile

The model presented considers Reynolds numbers less than 2100, which corresponds to laminar flow for fully developed flow in tubes. If a plug flow were assumed, a simpler solution could be deduced in terms of Bessel functions of order zero. However, a plug flow velocity profile would only be appropriate in the trachea or for turbulent flow. For this application a fully developed laminar velocity profile is more appropriate than a plug flow profile for radial mass transport, since in the real case the velocity at the wall of the daughter tube should be zero (no slip).

Based on the above arguments, a fully developed laminar (FDL) flow axial velocity distribution is used for V_z:

$$V_z = 2V_{\text{avg}}(1 - x^2), \tag{3}$$

where V_{avg} is the arithmetic average axial gas velocity over the tube cross section and x is dimensionless radial position, r/R.

In reality, the velocity distribution in each airway branch will not be fully developed over the entire branch due to the mechanical mixing at tube bifurcations induced by irregular axial velocity profiles and secondary flows. Scherer *et al.*[22] proposed accounting for these mixing effects by using an effective diffusivity in the form $\mathcal{D}_d = \mathcal{D} + 2KRV_{\text{avg}}$, where K is assumed to be uniform over the entire airway tree and dependent only upon the direction of axial flow. Scherer also assumed an ideal plug flow in a five-generation, glass tubing model of the bronchial airways, and determined K to be 1.08 for inspiration and 0.37 for expiration. Ultman and Blatman[24] determined analogous values of 1.48 and 0.50, respectively, based on so called ''developing'' and ''redeveloping'' dispersion theory, and concluded that Taylor dispersion was the dominant mechanism of mixing. In general, these relationships are applicable to one-dimensional models, which do not include radial diffusion. In our current study, the effective diffusivity is not incorporated into the steady-state diffusion equation, because radial diffusion is included, and, thus the effect of Taylor dispersion is included.[5]

Next, we define Pe_r as the radial Peclet number in the following fashion:

$$\text{Pe}_r = 2V_{\text{avg}}R/\mathcal{D}; \tag{4}$$

Pe_r represents the ratio of axial convective mass flux to radial diffusion, and may be expressed as $\text{Pe}_r = \text{Re}\,\text{Sc}$, where Re is the Reynolds number and Sc is the Schmidt number [0.56, 1.19, and 0.54 for NO, EtOH, and H_2O, respectively, diffusing in air at body temperature, ambient pressure, saturated (BTPS)]. In general, the Peclet number Pe represents the ratio of convective mass transport to diffusive mass transport. We could also define the axial Peclet number, $\text{Pe}_z = LV_{\text{avg}}/\mathcal{D}$, corresponding to axial convection/axial diffusion. However, in the problem which the current studies addresses, radial diffusion dominates axial diffusion; hence, the alternate formulation is more appropriate.

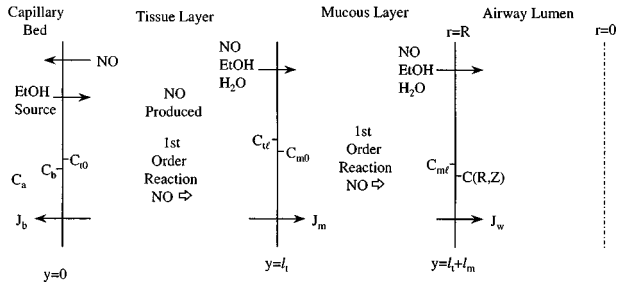

FIGURE 3. Detailed description of the gas exchange mechanism for transport of NO, EtOH, and H_2O through tissue and mucous layers to the airway lumen.

Diffusion, Consumption, and Generation in Tissue, Mucous, and Blood

As depicted in Fig. 2, the gas exchange mechanism in the conducting airways for endogenous gases includes diffusion through capillaries, tissue, and mucous, and the mucous/air interface. NO is generated in the tissue, consumed by substrates in the blood, tissue, and mucous, and diffuses into the airway lumen. EtOH present in the blood diffuses from the capillaries through the tissue and mucous into the airway lumen. No consumption or production of EtOH occurs in either the tissue or mucous. Within cellular tissue, H_2O is maintained at a nearly constant concentration. Hence, the primary mass transfer resistance to H_2O transport into the lumen is provided by the thin layer of mucous surrounding the airway wall. Figure 3 gives a schematic representation for the equivalent gas exchange network.

Several different airway cells serve as the source of NO, which is produced by the intracellular conversion of L-arginine to L-citrulline.[7,26] Although several chemical reactions occur in tissue and mucous which consume NO, most of these reactions are relatively slow at naturally occurring nitric oxide concentrations *in vivo*.[1,17,26] Therefore, it is assumed in this work that at physiological concentrations only the first order reactions are important.[1,7,16,26] NO diffuses through cell membranes to airway tissue and into either the airway lumen, or into blood capillaries, where it rapidly binds to hemoglobin.[1,20,26]

An effective first order rate constant in the tissue, κ_t, is defined to account for first order reactions, which allow the NO consumption rate per unit volume in tissue, G_t, to be expressed as $G_t = \kappa_t C_t$, where C_t is the concentration of NO in pulmonary tissue. The analogous first order reaction rate constant for consumption of NO in the mucous was set to $\kappa_m = \kappa_t/10$, based on the assumption that reactants consuming NO are at much lower concentrations in the mucous than in the tissue. Thus the NO consumption rate per unit volume in the mucous layer is expressed as $G_m = \kappa_m C_m$, where C_m is the concentration of NO in the mucous.

Mass transfer through the tissue and mucous layers is modeled by representing these layers as annuli of thicknesses, l_t and l_m, with diffusivities of $\mathcal{D}_t$ and $\mathcal{D}_m$, respectively. Hence the capillaries are modeled as a continuous annular sheet exterior to the tissue layer. At the boundaries between adjacent phases (i and j), partition coefficients relate the concentrations by $\lambda_{i:j} = C_i/C_j$. Diffusive flux is assumed to be continuous across each boundary.

GOVERNING EQUATION

Derivation

Neglecting angular diffusion, as well as angular and radial convection, the steady-state diffusion equation relates the gas phase concentration of the diffusing species, C, to the radial and axial coordinates, r and z, respectively, as follows:

$$V_z \frac{\partial C}{\partial z} = \mathcal{D}\frac{\partial^2 C}{\partial z^2} + \frac{\mathcal{D}}{r}\frac{\partial}{\partial r}\left(r\frac{\partial C}{\partial r}\right), \tag{5}$$

where V_z is the axial velocity and $\mathcal{D}$ is the gas phase diffusivity. The left-hand term of Eq. (5) represents axial convection, whereas the two terms on the right-hand side represent axial diffusion and radial diffusion, respectively.

Equation (5) is subject to the following boundary conditions:

$$(1)\quad C(r, z=0) = C_0, \tag{6}$$

$$(2)\quad C(r=0, z) = \text{finite}, \tag{7}$$

$$(3)\quad C(r, z\to\infty) = \text{finite}, \tag{8}$$

$$(4)\quad J_w = \mathcal{D}\left.\frac{\partial C}{\partial r}\right|_{R,z} = \lambda_{m:a}\lambda_{t:m}k_1(C_{\text{sat}} - C(r,z)), \tag{9}$$

where $\lambda_{m:a}$ and $\lambda_{t:m}$ are partition coefficients which relate the concentrations at the mucus:lumen and tissue:mucus boundaries, respectively, and k_1 is analogous to a film coefficient for the tissue and mucous layers. Boundary condition (1) is based on the assumption of uniform gas phase concentration at each branch inlet ($z = 0$). Here we assume that the presence of secondary flows,[29] even at very low Reynolds numbers, will induce some degree of mixing right at the entrance. Thus, a uniform concentration is a reasonable first approximation. Boundary condition (2) requires that the concentration must be bounded at the tube centerline,

TABLE 2. Tissue parameters used for all diffusing species.

Parameter	Species	Units	Central Value	Lower Limit[a]	Upper Limit[a]	Reference(s)
κ_t	NO	s^{-1}	0.346	0.0462	6.93	1, 7, 21
$\lambda_{m:a}$	NO	⋯	0.0416	0.0333	0.05	15
$\lambda_{m:a}$	EtOH	⋯	2000	⋯	⋯	9
$\lambda_{m:a}$	H_2O	⋯	20,000	⋯	⋯	8
$\lambda_{t:m}$	All[b]	⋯	1	0.8	1.2	9
$\lambda_{b:t}$	All[b]	⋯	1	0.8	1.2	9
$\mathcal{R}_p$	NO	s/cm	6000	3000	9000	10, 23
$\mathcal{R}_p$	EtOH	s/cm	6000	⋯	⋯	10, 23
$\mathcal{D}$	NO	cm^2/s	0.27	0.20	0.33	2
$\mathcal{D}$	EtOH	cm^2/s	0.13	⋯	⋯	3
$\mathcal{D}$	H_2O	cm^2/s	0.29	⋯	⋯	2
$\mathcal{D}_t$	NO	cm^2/s	2.0×10^{-5}	0.7×10^{-5}	3.3×10^{-5}	2
$\mathcal{D}_t$	EtOH	cm^2/s	0.56×10^{-5}	⋯	⋯	3
$\mathcal{D}_m$	NO	cm^2/s	3.0×10^{-5}	1.5×10^{-5}	4.5×10^{-5}	2
$\mathcal{D}_m$	EtOH	cm^2/s	1.6×10^{-5}	⋯	⋯	9
$\mathcal{D}_m$	H_2O	cm^2/s	1×10^{-5}	⋯	⋯	2
l_t[c]	NO	μm	100	80	120	6
l_m[c]	NO	μm	10	5	15	3
R[c]	NO	cm	0.61	0.49	0.73	25

[a]Upper and lower limits are for NO gas exchange uncertainty analysis in generation 1.
[b]Used for NO, EtOH, and H_2O.
[c]Used for NO gas exchange uncertainty analysis in generation 1 only.

and boundary condition (3) simply states that for an infinitely long tube some finite concentration (C_{sat}) will be reached within the gas phase.

The fourth boundary condition is a unique feature of this modeling study, and relates the mass flux as a linear function of concentration at the lumen wall. The fourth boundary condition also includes the solubility characteristics of the gas (valid for NO, EtOH, and H_2O). Equation (9) assumes that a steady-state concentration profile is established rapidly in the tissue and mucous layers (i.e., there are no transient effects between the source of C_{sat} and the lumen wall), and that the NO production rate in the tissue surrounding the lumen is constant.

Despite the similarities between Eqs. (1) and (9), they are independent equations. Equation (1) relates the diffusive flux, J_w, to the gas phase mass transfer coefficient, k_c, whereas Eq. (9) relates the J_w to properties of the mucous, tissue, and capillary bed, including the effective film coefficient, k_1.

For NO, the bulk concentration in the blood, C_a, is assumed to be approximately zero due to the rapid reaction with hemoglobin in blood capillaries. However, a finite mass transfer resistance between the tissue and the blood must be considered[10] and is defined by the constant, $\mathcal{R}_p$. $\mathcal{R}_p$ (in s/cm) influences the rate of mass transfer into the lumen, and can be estimated from the following equation: $\mathcal{R}_p = S/\dot{Q}$(s/cm) where S is the surface area (in cm^2) available for diffusion across the capillaries, and $\dot{Q}$ (in cm^3/s) is the blood flow rate to the capillaries.[10] Estimates of $\mathcal{R}_p$ for NO and EtOH are presented in Table 2. Then, the concentration at the tissue/lumen boundary (the airway wall) can be expressed in terms of the mass flux of the diffusing species at that boundary. Solution of steady-state mass balances for NO in the tissue and mucous layers thus leads to the following expression for k_1:

$$k_1 = \frac{\lambda_{t:m}K_b\beta_m\beta_t - \lambda_{t:m}v_t^2\beta_m + v_m^2(K_b+\beta_t)}{\lambda_{t:m}(\lambda_{t:m}K_b\beta_t - \lambda_{t:m}v_t^2 + \beta_m(K_b+\beta_t))}, \quad (10)$$

where $v_t = \sqrt{\kappa_t\mathcal{D}_t}$; $v_m = \sqrt{\kappa_m\mathcal{D}_m}$; $\beta_t = \sqrt{K_t^2 + v_t^2}$; $\beta_m = \sqrt{K_m^2 + v_m^2}$; $K_b = 1/(\lambda_{b:t}\mathcal{R}_p)$; $K_t = v_t/\sinh(l_t\sqrt{\kappa_t/\mathcal{D}_t})$; $K_m = v_m/\sinh(l_m\sqrt{\kappa_m/\mathcal{D}_m})$.

For an infinitely long tube, a state is approached at which there is no mass transfer into the gas phase. At this state, the gas phase concentration approaches C_{sat}. Both k_1 and C_{sat} depend upon the physical and chemical properties (diffusivity, partition coefficient, thickness, and reaction rate constant) in the tissue, mucous, and capillaries. In addition, for the gas exchange of NO, C_{sat} depends upon the NO production rate per unit volume, whereas k_1 does not. In general, the production rate of NO is not known, but C_{sat} is not required to determine k_c.

For EtOH, $C_{\text{sat}} = C_a/\lambda_{b:t}\lambda_{t:m}\lambda_{m:a}$, where C_a is the bulk concentration of EtOH in the blood, and k_1 is analogous to an overall mass transfer coefficient for the capillaries, tissue, and mucous layers,

$$k_1 = \frac{1}{\left(\frac{\mathcal{R}_p}{\lambda_{b:t}} + \frac{\lambda_{t:m} l_m}{\mathcal{D}_m} + \frac{l_t}{\mathcal{D}_t} \right)}. \tag{11}$$

For H_2O, $C_{sat} = C_{tl}/\lambda_{t:m}\lambda_{m:a}$, where C_{tl} is the concentration of H_2O in the tissue (assumed constant), and k_1 is analogous to a film coefficient for the mucous layer,

$$k_1 = \frac{\mathcal{D}_m}{\lambda_{t:m} l_m}. \tag{12}$$

Solution

Defining the following dimensionless variables:

$$\theta = (C(r,z) - C_{sat})/(C_0 - C_{sat}), \tag{13}$$

$x = r/R$, and $\xi = z/R\,\mathrm{Pe}_r$, and substituting Eqs. (3) and (4), the governing equation [Eq. (5)] is written in dimensionless form as

$$(1-x^2)\frac{\partial \theta}{\partial \xi} = \frac{1}{Pe_r^2}\frac{\partial^2 \theta}{\partial \xi^2} + \frac{1}{x}\frac{\partial}{\partial x}\left(x \frac{\partial \theta}{\partial x} \right). \tag{14}$$

Transforming the boundary conditions in terms of the dimensionless variables

$$(1)\quad \theta(x, \xi = 0) = 1, \tag{15}$$

$$(2)\quad \theta(x = 0, \xi) = \text{finite}, \tag{16}$$

$$(3)\quad \theta(x, \xi = \infty) = \text{finite}, \tag{17}$$

$$(4)\quad \frac{\partial \theta}{\partial x}(x = 1, \xi) + \alpha\,\theta(x = 1, \xi) = 0. \tag{18}$$

Since k_c is independent of C_{sat}, its dependence upon properties of the tissue, mucous, and capillary bed are conveniently described by the dimensionless film coefficient, α,

$$\alpha = \lambda_{m:a}\lambda_{t:m} R k_1 / \mathcal{D}. \tag{19}$$

Note that α is directly proportional to $\lambda_{m:a}$. Thus, α increases monotonically with the solubility of the diffusing species.

The solution of Eq. (14) is obtained by the classical method of separation of variables. The general solution to Eq. (14) is

$$\theta = \sum_{n=1}^{\infty} A_n e^{-\gamma_n^2 \xi} e^{-\eta_n/2} M(a_n; 1; \eta_n), \tag{20}$$

where $\eta_n = \gamma_n x^2$. γ_n are the eigenvalues, M is the confluent hypergeometric function, A_n the series coefficients, and a_n is defined as

$$a_n = \frac{1}{2} - \frac{\gamma_n}{4}\left[1 + \left(\frac{\gamma_n}{\mathrm{Pe}_r} \right)^2 \right]. \tag{21}$$

In general, both A_n and γ_n depend only on α and Pe_r.

For the special case of ideal FDL flow (without axial diffusion), computation is simplified considerably, since the eigenvalues depend only on α and become independent of Pe_r. In theory, this approximation is only valid for NO gas exchange in the upper airways (between generations 1 and 7). However, boundary layer theory[2] predicts that gas phase mass transfer coefficients for generations 1–7 may be influenced by skewed velocity profiles and secondary flows that arise due to the bifurcations between airway branches. Bird *et al.*[2] stated that an ''entrance length'' on the order of $0.035D\,\mathrm{Re}$ is required to build up a parabolic FDL velocity profile. On this basis, an ideal FDL velocity distribution assumption would not be valid until at least the eighth generation (i.e., for Re less than about 50).

Mass Transfer Coefficient: Calculation

For each specific generation of the pulmonary airways an average mass transfer coefficient, $\overline{k_c}$, is determined by integrating Eq. (1) over the length of the branch, L, and applying the generalized mean value theorem to k_c. This is appropriate because a more detailed gas exchange model will perform a numerical integration over each branch. The result is

$$\overline{k_c} = \left(\frac{\mathcal{D}}{R} \right) \frac{\int_0^{\xi_L} \frac{\partial \theta}{\partial x}(1, \xi)\, d\xi}{\int_0^{\xi_L} (\theta(1,\xi) - \overline{\theta(\xi)})\, d\xi}, \tag{22}$$

where

$$\xi_L = \frac{L}{R\,\mathrm{Pe}_r}; \tag{23}$$

$\overline{\theta(\xi)}$ is the average or bulk gas phase concentration determined from Eqs. (2) and (13), which upon substitution into Eq. (20) is expressed as

$$\overline{\theta}(\xi) = 2\int_0^1 \theta(x,\xi)x\,dx$$

$$= \sum_{n=1}^{\infty} A_n e^{-\gamma_n^2 \xi} e^{-\gamma_n/2}$$

$$\times \sum_{m=0}^{\infty} \frac{(a_n)_m \gamma_n^m}{(2)_m m!} M(1; m+2; \gamma_n/2). \quad (24)$$

Results are expressed in terms of the local Sherwood number, Sh(z), a dimensionless form of k_c defined by

$$\mathrm{Sh}(\xi) = Dk_c(\xi)/\mathcal{D}. \quad (25)$$

Similarly, the average Sherwood number, $\overline{\mathrm{Sh}}$ is defined as

$$\overline{\mathrm{Sh}}(\xi_L) = D\overline{k_c}(\xi_L)/\mathcal{D}. \quad (26)$$

Equating J_w in Eqs. (1) and (9), solving for k_c, substituting the result into Eq. (25), and using the appropriate definitions of the dimensionless variables, the following expression is derived for Sh(ξ):

$$\mathrm{Sh}(\xi) = \frac{-2\alpha\theta(1,\xi)}{\theta(1,\xi) - \overline{\theta}(\xi)}. \quad (27)$$

By substituting the solutions from Eqs. (20) and (24) into Eq. (27), the following expression is obtained for Sh(ξ):

$$\frac{\mathrm{Sh}(\xi)}{2\alpha} = \frac{\Sigma_{n=1}^{\infty} A_n e^{-\gamma_n^2\xi} e^{-\gamma_n/2} M(a_n;1;\gamma_n)}{\Sigma_{n=1}^{\infty} A_n e^{-\gamma_n^2\xi} e^{-\gamma_n/2}\left[\Sigma_{m=0}^{\infty} \frac{(a_n)_m \gamma_n^m}{(2)_m m!} M\left(1; m+2; \frac{\gamma_n}{2}\right) - M(a_n;1;\gamma_n)\right]}. \quad (28)$$

Similarly, an expression for $\overline{\mathrm{Sh}}$ is obtained by combining Eqs. (20), (22), (24), and (26), and integrating:

$$\frac{\overline{\mathrm{Sh}}(\xi_L)}{2\alpha} = \frac{\Sigma_{n=1}^{\infty} A_n \frac{(1-e^{-\gamma_n^2\xi_L})}{\gamma_n^2} e^{-\gamma_n/2} M(a_n;1;\gamma_n)}{\Sigma_{n=1}^{\infty} A_n \frac{(1-e^{-\gamma_n^2\xi_L})}{\gamma_n^2} e^{-\gamma_n/2}\left[\Sigma_{m=0}^{\infty} \frac{(a_n)_m \gamma_n^m}{(2)_m m!} M\left(1; m+2; \frac{\gamma_n}{2}\right) - M(a_n;1;\gamma_n)\right]}. \quad (29)$$

The above model was used to compute Sh(ξ) and $\overline{\mathrm{Sh}}$ for airway geometries (i.e., L/D) typical of the first 17 generations and flow conditions [tracheal flows of 5×10^{-5} m–5×10^{-4} m s^{-1} (50–500 cm^3 s^{-1}) corresponding to a tracheal Re between 200 and 2100]. Numerical calculations were performed with the aid of a MICROSOFT EXCEL® Spreadsheet. Since the NO production rate was considered an unknown parameter, detailed gas phase concentration profiles were not computed.

PARAMETER VALUES AND UNCERTAINTY ANALYSIS

Inspection of Eq. (29) reveals that $\overline{\mathrm{Sh}}$ depends only on α, Pe_r, and $(L/R) = 2(L/D)$. Since Pe_r and (L/D) depend only upon flow conditions, lumen geometry, and the gas phase diffusivity, α completely describes the functional dependence of $\overline{\mathrm{Sh}}$ in terms of properties of the tissue, mucous, and capillary bed. Those parameters that influence α include κ_t, $\lambda_{m:a}$, $\lambda_{b:t}$, $\lambda_{t:m}$, $\mathcal{R}_p$, $\mathcal{D}$, $\mathcal{D}_t$, $\mathcal{D}_m$, l_m, l_t, and R (or D), which will be henceforth referred to as ''tissue'' properties. The gas phase diffusivity of NO, EtOH, and water are all well characterized and will not be considered in the uncertainty analysis. The effect of flow conditions and lumen geometry will be considered independently with the lumped parameter $\mathrm{Pe}_r(D/L)$. Thus, our uncertainty analysis will focus on the variation of $\overline{\mathrm{Sh}}$ on α. This is done by first estimating upper and lower limits for α based on the uncertainties of $\lambda_{m:a}$, $\lambda_{t:m}$, κ_t, and other properties of the tissue layers surrounding the lumen (see Table 2).

The effective first order rate constant in the tissue, κ_t, exhibits the widest range of uncertainty due to the broad range of probable half-lives for NO. Based on Beckman and Koppenol,[1] the half-life of NO in tissue, $t_{1/2}$, is on the order of 1 s; however, the probable range is between 0.1 and 15 s.[7,21,28] $t_{1/2}$ was varied over its range of

TABLE 3. Lower and upper limit (α_{LL} and α_{UL}) for NO gas exchange uncertainty analysis (for generation 1 only).

Parameter	α_{LL}	α_{UL}	$100\%\times[(\alpha_{LL}/\alpha_{CV})-1]$[a]	$100\%\times[(\alpha_{UL}/\alpha_{CV})-1]$[a]
κ_t	0.52×10^{-4}	8.1×10^{-4}	−75	294
$\lambda_{m:a}$	1.6×10^{-4}	2.5×10^{-4}	−20	20
$\lambda_{t:m}$	1.7×10^{-4}	2.4×10^{-4}	−18	18
$\lambda_{b:t}$	2.1×10^{-4}	2.0×10^{-4}	0.3	−0.2
$\mathcal{R}_p$	2.1×10^{-4}	2.0×10^{-4}	1.8	−0.2
$\mathcal{D}$	2.8×10^{-4}	2.8×10^{-4}	36	−17
$\mathcal{D}_t$	1.4×10^{-4}	2.4×10^{-4}	−32	15
$\mathcal{D}_m$	1.9×10^{-4}	2.1×10^{-4}	−6.7	2.9
I_t	2.2×10^{-4}	1.9×10^{-4}	4.8	−6.9
I_m	2.1×10^{-4}	2.0×10^{-4}	3.4	−2.6
R	1.7×10^{-4}	2.5×10^{-4}	−17	24

[a]Percent of deviation of α_{LL} and α_{UL} from the central value ($\alpha_{CV}=2.04\times10^{-4}$).

probable values, 0.1–15 s, with $t_{1/2}=2$ s selected as a base value. κ_t was then calculated from the half-life of NO in pulmonary tissue from $\kappa_t=\ln(2)/t_{1/2}$.

The uncertainty analysis on α is only performed for gas exchange of NO in the first generation. We did not explore the sensitivity of $\overline{Sh}$ on α for other compounds, such as EtOH and water, because their partition coefficients are well characterized, and are inert (i.e., $\kappa_t=0$) in the bronchial mucosal tissue.

Table 3 shows values of α determined in the uncertainty analysis for NO gas exchange in generation 1. All values displayed in Table 3 are for the first generation, where the central value, α_{CV}, is 2.04×10^{-4}. Values determined at the upper and lower limits of the corresponding tissue parameters are denoted α_{UL} and α_{LL}, respectively. As κ_t is varied between its upper and lower limits, α varies between 294% and −75%, respectively, of its central value. For all of the other parameters, the maximum variation in α is only 36%. Hence, κ_t determined the upper and lower bounds of α for the uncertainty analysis.

$\overline{Sh}$ values for EtOH and water gas exchange were computed for the same generations and range of flow conditions used for NO gas exchange with all parameters at their central values (see Table 2). Although the functional dependence of $\overline{Sh}$ upon Pe_r, (L/D) and α is the same for both EtOH and NO, $\lambda_{m:a}$ is nearly 50,000 times larger for EtOH. Hence, at any given Pe_r and (L/D) the corresponding value of α will be much larger for EtOH than for NO. Therefore, differences in the dependence of $\overline{Sh}$ upon Pe_r and (L/D) between NO and EtOH can be attributed to differences in α. For H_2O, $\lambda_{m:a}$ is about 10 times larger than for EtOH.

RESULTS

Local Sherwood Number

For NO gas exchange, $Sh(z)$, was found to approach an asymptotic value (for a very long tube) of 6, which is consistent with the results of George *et al.*[10] and Grotberg.[11] Sh approaches its asymptotic value more rapidly at low Pe_r. Figure 4(a) shows the dependence of Sh on axial distance-to-radius ratio (z/R) at a tracheal flow (Q_{tr}) of $2\times10^{-4}\,m^3\,s^{-1}$ ($200\,cm^3\,s^{-1}$) for NO gas exchange with all parameters at their central values. For the main bronchi (generation 1, $Pe_r=397$), $(z/R)\rightarrow0$, Sh $\rightarrow\infty$, as shown in Fig. 4(a). For the human pulmonary airways, (L/D) ranges between about 1.5 and 4 (see Table 1). In generation 1, Sh does not approach its asymptotic value in the first generation. However, by generation 10, at $Pe_r=7.2$, Sh rapidly approaches its asymptotic value. For NO this trend continues through generation 17 (the limit of bronchioles) for $Pe_r=0.13$. Thus, at high Pe_r, Sh is maintained at larger values due to the effects of axial convection. As Pe_r decreases, axial convection becomes less important and Sh rapidly approaches its asymptotic value.

For EtOH gas exchange, the trend is qualitatively similar at high Pe_r. However, the asymptotic value becomes more sensitive to changes in Pe_r. Figure 4(b) shows the dependence of Sh on z/R at $Q_{tr}=2\times10^{-4}\,m^3\,s^{-1}$ ($200\,cm^3\,s^{-1}$) for EtOH gas exchange. For generation 1 ($Pe_r=842$), the Sh values are slightly higher than the corresponding values for NO. For generation 10 at $Pe_r=15.4$, Sh approaches an asymptotic value of 6.0, and the Sh values are nearly the same as the corresponding values for NO near the entry of the tube. By generation 17, at $Pe_r=0.28$, Sh approaches an asymptotic value of 7.1 for large (z/R). Hence, the asymptotic value of Sh increases as Pe_r decreases for EtOH gas exchange. Note that these results for EtOH at $Q_{tr}=2\times10^{-4}\,m^3\,s^{-1}$ ($200\,cm^3\,s^{-1}$) are not directly comparable to the corresponding results for NO and H_2O, because the Schmidt number, Sc, is nearly twofold higher for EtOH than for NO and H_2O. As a result, $Pe_r=Re\,Sc$ will be about twice as large at the same flow rate (i.e., at the same Re).

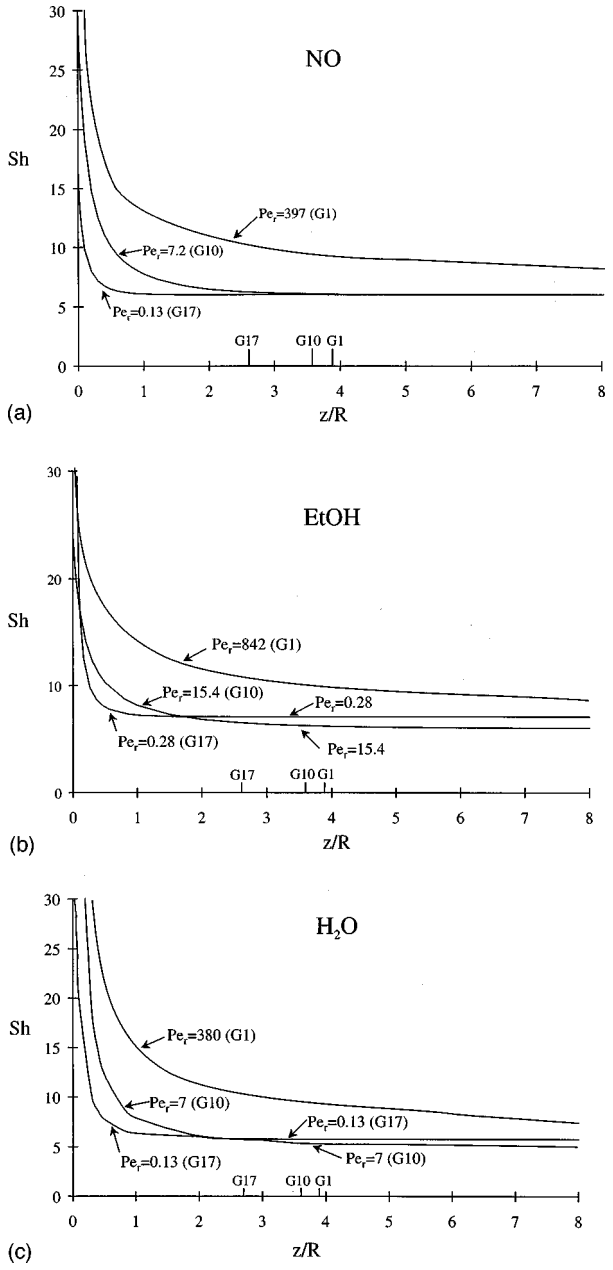

FIGURE 4. Model prediction for the local Sh vs z/R at varying flow rates and thus Pe_r. (a) NO gas exchange ($t_{1/2}$ = 2 s). (b) EtOH gas exchange. (c) H_2O gas exchange. G1: generation 1; G10; generation 10; G17: generation 17.

For H_2O gas exchange, Fig. 4(c) shows the dependence of Sh on z/R at $Q_{tr}=2\times10^{-4}\,m^3\,s^{-1}$ (200 $cm^3\,s^{-1}$). For generation 1 ($Pe_r=380$), the Sh values are higher than the corresponding values for NO for $(z/R)<3$. Although, for generation 10 at $Pe_r=7$, Sh approaches an asymptotic value of 5.5 as $(z/R)\rightarrow\infty$, the Sh values are significantly higher than the corresponding values for NO near the entry of the tube. By generation 17 at $Pe_r=0.13$, Sh approaches an asymptotic value of 6.0 for large (z/R). Hence, like for EtOH, the asymptotic value of Sh increases as Pe_r decreases for H_2O gas exchange. This behavior is the result of axial diffusion, which enhances the mass transfer coefficient at low Pe_r for highly soluble gases and will be discussed in greater detail below.

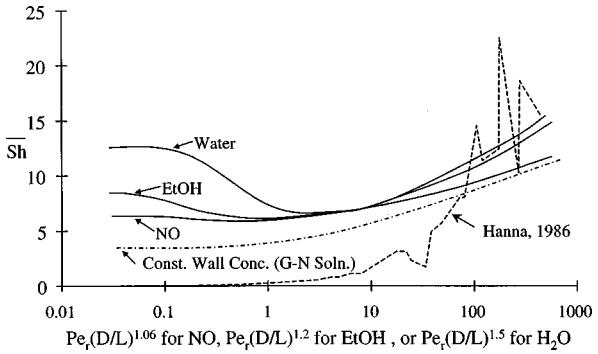

FIGURE 5. Model prediction of $\overline{Sh}$ vs $Pe_r(D/L)^n$ for NO, EtOH, and H_2O. The dashed line is the correlation proposed by Hanna and Scherer (Ref. 13) for inhalation. The center line is the Graetz–Nusselt solution for constant wall concentration.

Average Sherwood Number

For each of the three diffusing species considered, $\overline{Sh}$ is a function of Pe_r and (L/D) for the model described above. $\overline{Sh}$ increases with Pe_r due to the effects of axial convection and decreases with (L/D) due, in part, to axial diffusion (see Fig. 4). For Pe_r $D/L>10$, the effects of axial diffusion become less important. With no axial diffusion, $\overline{Sh}$ is a smooth function of the lumped variable Pe_r D/L. Irregularities in plots of $\overline{Sh}$ vs Pe_r D/L, with axial diffusion included, indicated that $\overline{Sh}$ has a separate functional dependence on Pe_r and L/D, and therefore could not be expressed simply as a function of the single variable Pe_r D/L. However, we can obtain a smooth functional relationship by expressing $\overline{Sh}$ in terms of a lumped variable of the form $Pe_r(D/L)^n$, where n is a constant $(n>1)$. This modified dependence on D/L is primarily due to the greater relative effect of axial diffusion for short tubes, which becomes more important as the solubility of the diffusing species in tissue increases (see Fig. 4). The values of n were estimated at 1.06, 1.2, and 1.5, for NO, EtOH, and water vapor, respectively.

Figure 5 shows the model results for $\overline{Sh}$ vs $Pe_r(D/L)^n$ (log scale) for NO, EtOH, and H_2O. For all three gases, $\overline{Sh}$ passes through a minimum at an intermediate value of $Pe_r(D/L)$, the result of an enhanced mass transfer coefficient at low Pe_r. The minimum is barely detectable for NO, but becomes much more exaggerated as the solubility of the gas increases in the case of EtOH and H_2O. The curves for NO and EtOH lie very close to

TABLE 4. Parameters for correlation of $\overline{Sh}$ with $Pe_r(D/L)^n$.

Species	N	m	b	B_0	B_1	B_2	B_3	r^2
No axial diffusion								
NO	1.0	0.67	⋯	6	0	0.083	0.052	0.999
With axial diffusion								
NO	1.06	0.82	0.32	5.5	0.7	0.26	0.16	0.96
EtOH	1.2	0.72	0.12	5.6	2.9	0.2	0.14	0.97
H_2O	1.5	0.67	0.18	5.6	7.4	0.17	0.13	0.94

each other at intermediate $Pe_r(D/L)^n$. As $Pe_r\ D/L \to 0$, $\overline{Sh}$ approaches an apparent asymptote of 6.2 for NO, compared to about 8.5 for EtOH and about 13 for H_2O. Since EtOH and water are more soluble in tissue than NO by roughly four and six orders of magnitude, respectively, these differences are attributed to corresponding differences in α. For H_2O, the $\overline{Sh}$ values are significantly larger than those for both NO and EtOH at nearly all values of $Pe_r\ D/L$.

Also shown in Fig. 5 is the correlation of Hanna and Scherer[13] (computed using the Sc number for NO) which was based on measurements of local mass transfer coefficients in a cast replica of the upper respiratory tract which included the nasal cavity through the distal trachea,[12] as well as the classical Graetz–Nusselt solution at a constant wall concentration. Hanna and Scherer's relationship (for inhalation) is $\overline{Sh} = 0.045\ Re^{0.856}\ Sc^{1/3}$. As might be expected, their correlation is in good agreement with our model results for $Pe_r(D/L)^n > 100$ (i.e., in the upper airways where Hanna and Scherer's correlations are valid). However, for $Pe_r(D/L)^n < 100$ their correlation predicts $\overline{Sh} \to 0$ as $Pe_r(D/L)^n \to 0$, while our model predicts that $\overline{Sh}$ tends towards a finite value (this value depends on the solubility of the gas) as $Pe_r(D/L)^n \to 0$. The classical Graetz–Nusselt solution shows values of $\overline{Sh}$ which are generally about 30% lower than our model results. In addition, this solution is a monotonically decreasing function of $Pe_r(D/L)^n$ because axial diffusion is not considered.

In order to place these results in a more tractable form for use in gas exchange models, $\overline{Sh}$ was correlated with Pe_r and length-to-diameter ratio (L/D) using the method of least squares for each branch in generations 1–17 (the limit of bronchioles) and Q_{tr} in the range $5 \times 10^{-5}\ m\ s^{-1}$ to $5 \times 10^{-4}\ m\ s^{-1}$ (50–500 $cm^3\ s^{-1}$) using the following form:

$$\overline{Sh} = B_0 + B_1[1 - \exp(-b/(Pe_r(D/L)^n))] + \frac{B_2\ Pe_r(D/L)^n}{1 + B_3(Pe_r(D/L)^n)^m}. \quad (30)$$

The first and third terms on the right-hand side of Eq. (30) were developed following Eckert and Drake's solution for flow in tubes,[4,18] and the second (exponential) term was added to the empirical correlation to account for the minimum value which $\overline{Sh}$ passes through at intermediate $Pe_r(D/L)^n$. For high $Pe_r(D/L)^n$ this exponential term becomes insignificant, whereas it approaches B_1 as $Pe_r(D/L)^n \to 0$.

The parameters determined for the correlation of $\overline{Sh}$ were tabulated (Table 4). These correlations are valid under the following conditions: $0.06 < Re < 2300$ and $1.36 < (L/D) < 3.92$. Using the central value $\kappa_t = 0.347\ s^{-1}$ ($t_{1/2} = 2$ s) to account for consumption of NO in tissue, values of $\overline{Sh}$ were determined for NO and correlated. The value for B_0 is approximately equal to the minimum value of $\overline{Sh}$ and the sum $B_0 + B_1$ was forced to be equal to the value of $\overline{Sh}$ obtained at the minimum value of $Pe_r(D/L)^n$ [i.e., the apparent asymptotic value of $\overline{Sh}$ as $Pe_r(D/L)^n \to 0$.] This apparent asymptotic value was equal to 6.2, 8.5, and 13 for NO, EtOH, and water, respectively. The remaining parameters in the correlation were chosen iteratively until a minimum in the sum of squares of the error was achieved. The correlation coefficients (r^2) shown in Table 4 are all close to 1; hence, the correlations match the model results to within a maximum error of approximately 10%.

A limiting case to consider in our model results occurs for $[Pe_r(D/L)^n] \gg B_3^{-1/m}$ (e.g., for very high flow and a relatively short tube). Under these conditions, the form of the correlation [Eq. (30)] reduces to

$$\overline{Sh} = B_0 + (B_2/B_3)[Pe_r(D/L)^n]^{1-m}, \quad (31)$$

which is analogous to the Leveque solution for mass transfer between a fixed surface and a semi-infinite fluid flowing over the surface with a linear velocity profile and no slip at the surface.[19] If axial diffusion is neglected, the exponents, $(1-m)$ and n, are equal to the accepted values of 0.33 and 1, respectively, for FDL flow.[18] When axial diffusion is included, $1-m$ ranges from 0.18 (for NO) to 0.33 (for H_2O). The ratio B_2/B_3 is 1.6 when axial diffusion and dispersion are neglected,

TABLE 5. Variation of $\overline{Sh}$ for NO gas exchange.

Pe_r	L/D	Generation	$\overline{Sh}_{t_{1/2}=2\ s}$[a]	$\overline{Sh}_{t_{1/2}\to\infty}$[a]	$\overline{Sh}_{t_{1/2}=0.01\ s}$[a]
1000	3.90	1	9.56	9.57	9.53
500	2.29	2	9.44	9.43	9.40
100	1.36	3	8.46	8.44	8.48
50	3.54	5	6.99	6.98	7.00
10	3.11	10	6.13	6.14	6.13
1	3.11	14	6.03	6.03	6.04
0.04	2.61	17	6.19	6.17	6.52

[a]Half-life, $t_{1/2}$, in tissue. $t_{1/2}=2$ s, ∞, and 0.01 s correspond to $\kappa_t=0.347\ s^{-1}$, 0, and 69.3 s^{-1}, respectively.

compared to 1.6, 1.4, and 1.3 for NO, EtOH, and H_2O when axial diffusion is included, respectively.

In the uncertainty analysis for NO gas exchange, $\overline{Sh}$ was determined for values of κ_t at 0 (no reaction or $t_{1/2}\to\infty$) and 69 s^{-1} ($t_{1/2}=0.01$ s) for various conditions and compared with $\overline{Sh}$ at the central value of κ_t (0.347 s^{-1} corresponding to $t_{1/2}=2$ s). These results are displayed in Table 5. At any given Pe_r, the values of $\overline{Sh}$ for NO gas exchange are all within 1% of each other, except at $Pe_r=0.04$ (generation 17) where $\overline{Sh}$ at $t_{1/2}=0.01$ s is noticeably larger (6.52) than the corresponding $\overline{Sh}$ values at $t_{1/2}=2$ s and $t_{1/2}\to\infty$, 6.19 and 6.17, respectively. Because κ_t is the tissue property which most significantly influences α for NO gas exchange, it is inferred that $\overline{Sh}$ is insensitive to the physical and chemical properties, and to the geometry of the tissue, mucous, and capillary bed over the ranges considered in this study. However, as $Pe_r\to 0$, $\overline{Sh}$ departs slightly from the expected asymptotic value of 6.2. This effect becomes more pronounced for higher values of α.

DISCUSSION

The effect of bifurcations on flow patterns is complex. These complex flow patterns, and their effects on *radial* mass transfer, have not been accounted for in this or previous studies, and could significantly impact the results described above. Hence, the model described above represents only a crude first approximation. Results from this model, although quantitative in nature, are meant to provide a possible qualitative understanding of this complex phenomenon. A more detailed description of the actual flow patterns will be necessary to fully characterize the effect of bifurcations on radial mass transfer. Nonetheless, the results of the model are quite interesting and several points deserve further discussion.

If we consider the case where the diffusing species is transported from the tissue into the lumen as the gas flows through the branch, the concentration in the lumen will increase as the axial coordinate, z, increases. Therefore, the axial diffusive flux will be in the negative z

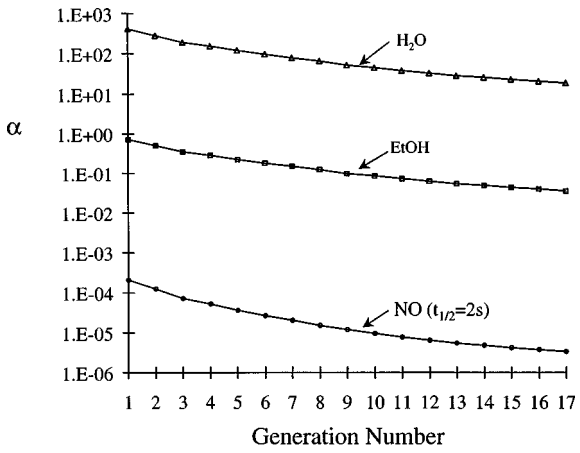

FIGURE 6. Values for α used in model predictions for NO (central value), EtOH, and water.

direction (opposite to the direction of bulk gas flow). Hence, axial diffusion will decrease the concentration near the end of the branch (increasing the concentration gradient, thereby enhancing mass transfer) and increase the concentration near the entrance of the branch (decreasing the concentration gradient, and hindering mass transfer).

The dimensionless parameter, α, represents the ratio of gas phase mass transfer resistance to mucous/tissue/capillary mass transfer resistance. α increases with increasing solubility of the diffusing species in the tissue and mucous layers. The values of α used to compute Sherwood numbers for gas exchange of NO (central value), EtOH, and H_2O are shown in Fig. 6 for each generation of the conducting airways. For diffusing species, which are sparingly soluble (e.g., NO), α is small, implying that the mucous/tissue/capillary mass transfer resistance is relatively large. For EtOH, α is much larger, and for H_2O, α very large, owing to the higher solubility of these two species; hence, the mucous/tissue/capillary mass transfer resistance is relatively small. Thus, mass transfer is limited by the mucous, tissue, and/or capillary bed for NO, and primarily by the gas phase for EtOH and water. Axial diffusion enhances mass transfer by increasing the concentration difference between the lumen wall and the bulk gas phase. Axial convection has the same effect, but transports the diffusing species in the opposite direction. For a high bulk gas velocity (large Pe_r), axial convection dominates and has the greatest impact upon Sh, whereas for low bulk gas velocity (small Pe_r) axial diffusion dominates. If α is small (e.g., for NO), the concentration gradient is greatest in the mucous, tissue, and/or capillary bed. Therefore, the enhancement of mass transfer due to axial diffusion is small, because gas phase resistance is small. When α is large, however, the concentration gradient (and hence resistance) is greatest in the gas phase, and the enhance-

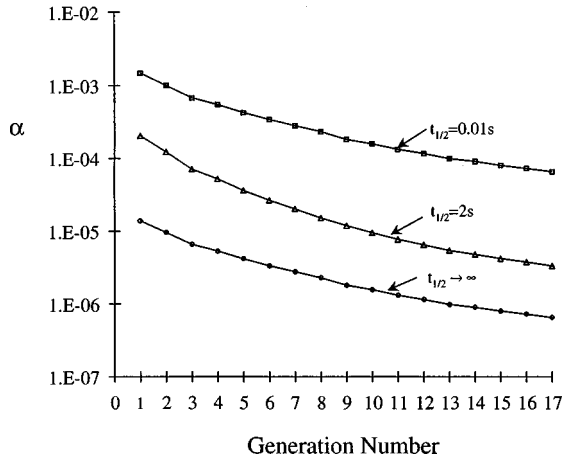

FIGURE 7. Values for α for NO gas exchange determined for values of κ_t at 0 (no reaction or $t_{1/2}\to\infty$), 69 s^{-1} ($t_{1/2}$ = 0.01 s), and at the central value of κ_t = 0.347 s^{-1} (corresponding to $t_{1/2}$ = 2 s).

ment of mass transfer due to axial diffusion becomes more significant.

In the scope of this study, α lies in the range of 6.5×10^{-7} and 1.49×10^{-3} (see Fig. 7) for NO, and Pe_r is between 0.04 and 1000. At the upper limit of Pe_r, the effects of axial convection is sufficient to increase $\overline{Sh}$ nearly twofold over the asymptotic value of 6.2 at the highest flow condition, $Q_{tr}=5\times10^{-4}\,m^3\,s^{-1}$ (500 $cm^3\,s^{-1}$) in the upper airways. However, since α is very small, the effect of axial diffusion upon $\overline{Sh}$ is insignificant as $Pe_r\to0$. As a result, $\overline{Sh}$ appears to approach an asymptotic value for $\overline{Sh}$ of 6.2 that is practically independent of α.

For EtOH and H_2O, α lies in the range of 0.0355–416 (see Fig. 6), and Pe_r is between 0.04 and 2000. As is the case for NO, the effects of axial convection is sufficient to increase $\overline{Sh}$ significantly over the asymptotic value at the highest flow rates and in the upper airways. In contrast to NO, axial diffusion significantly impacts $\overline{Sh}$ for EtOH and H_2O as $Pe_r\to0$, because α is relatively large. At the higher flow rates, axial convection dominates and $\overline{Sh}$ decreases as $Pe_r(D/L)^n$ decreases due to the dependence of axial convection upon gas velocity. This trend continues until axial diffusion begins to become important. Near $Pe_r(D/L)^n=1$, $\overline{Sh}$ reaches a minimum (see Fig. 5), because the axial diffusion term does not depend on velocity. Although the convection term becomes negligible relative to the diffusion term, the absolute value of the second derivative, $\partial^2C/\partial z^2$, continues to be an inverse function of the velocity which distorts the axial concentration gradient. Therefore, as Pe_r decreases further, the relative magnitude of axial diffusion increases, thereby increasing the average radial concentration gradient, enhancing mass transfer, and thus increasing $\overline{Sh}$. The overall result is that the $\overline{Sh}$ vs $Pe_r(D/L)^n$ plot passes through a minimum in the intermediate airways.

The assumption of first order consumption reactions occurring in the tissue and mucous may not be valid if NO is exogenously administered. Endogenous production of NO in tissue generates NO concentrations on the order of 10 ppb. When NO is exogenously administered at much higher concentrations (100 ppm), second order reactions, such as reaction of NO with oxygen or thiols,[27] may become significant.

The analysis described in this work is not limited to the gas exchange of endogenously produced gases in the pulmonary airways, but could be applied to a wide range of heat and mass transfer problems involving laminar flow in tubes. For example, Eq. (5) could be replaced by the steady-state heat equation and the analysis could be repeated for annular layers exhibiting thermal resistance surrounded by an isothermal heat source, resulting in a correlation for Nusselt number in terms of Re, L/D, and the Prandtl number. This analogy between heat and mass transfer may also provide an avenue for investigating this phenomenon experimentally.

CONCLUSION

Based on the results of this study, the maximum variation of $\overline{Sh}$ from its minimum value is roughly twofold in the conducting airways. Values of $\overline{Sh}$ predicted from the model presented in this study can be correlated in terms of a lumped variable, $Pe_r(D/L)^n$, where n is determined from model results. For diffusing species which are sparingly soluble in the tissue and mucous layers, such as NO, $\overline{Sh}$ is insensitive to the physical and chemical properties of the tissue and mucus (i.e., it is dependent only upon lumen geometry, gas phase properties, and flow conditions), and is insensitive to axial molecular diffusion at low Pe_r. In contrast, for more soluble species (e.g., EtOH and H_2O), $\overline{Sh}$ is sensitive to properties of the tissue and mucous, and is significantly influenced by molecular axial diffusion as $Pe_r\to0$. For all three gases $\overline{Sh}$ passes through a minimum at an intermediate value of $Pe_r(D/L)^n$ due to the effects of axial diffusion. The relative magnitude of axial diffusion increases as the solubility of the gas increases. The correlations developed in this study are useful for estimating gas phase mass transfer coefficients in the pulmonary conducting airways for use in more detailed gas exchange models. However, it may be of further interest to incorporate the solubility of the diffusing species into these correlations. Additional theoretical and experimental studies are necessary to fully characterize the effects of mixing and of secondary flows arising at bifurcations upon $\overline{Sh}$.

ACKNOWLEDGMENTS

This work was supported, in part, by a grant from the National Science Foundation (BES-9619340), a grant from the Committee on Research at the University of California, Irvine, and by generous start-up funds to one of the authors (S.C.G.) from the Department of Chemical and Biochemical Engineering and Materials Science at the University of California, Irvine.

NOMENCLATURE

A_n	series coefficients in analytical solution
$C(r,z)$	gas phase concentration of the diffusing species (mol/cm^3)
$\overline{C}(z)$	the average or bulk gas phase concentration (mol/cm^3)
C_a	bulk concentration in the blood (mol/cm^3)
C_b	concentration in blood at tissue interface (mol/cm^3)
C_m	concentration in mucous (mol/cm^3)
C_{m0}	concentration in mucous at tissue interface (mol/cm^3)
C_{ml}	concentration in mucous at airway wall (mol/cm^3)
C_{sat}	saturation concentration approached in gas phase as $z\rightarrow\infty$ (mol/cm^3)
C_t	concentration in tissue (mol/cm^3)
C_{t0}	concentration in tissue at capillary bed boundary (mol/cm^3)
C_{tl}	concentration in tissue at mucous interface (mol/cm^3)
C_0	gas phase concentration of the diffusing species at branch inlet, $z=0$ (mol/cm^3)
D	diameter of the airway branch (cm)
$\mathcal{D}$	gas phase diffusivity (cm^2/s)
$\mathcal{D}_m$	diffusivity in mucous (cm^2/s)
$\mathcal{D}_t$	diffusivity in tissue (cm^2/s)
$\mathcal{D}_d$	$\mathcal{D}+2KRV_{\text{avg}}$, effective diffusivity (cm^2/s)
G	NO consumption rate per unit volume in tissue (mol/cm^2 s)
k_c	local gas phase mass transfer coefficient (cm/s)
$\overline{k_c}$	average gas phase mass transfer coefficient (cm/s)
k_1	effective film coefficient for the tissue and mucous layers (cm/s)
K	constant relating $\mathcal{D}_d$ to $\mathcal{D}$ and Pe_r (1 for inspiration and 0.33 for expiration)
J	diffusive flux (mol/cm^2 s)
l	thickness of tissue or mucous layer (cm)
L	length of airway branch (cm)
M	Confluent hypergeometric function
n	constant exponent ($n>1$) or index for summation (integer)
Pe_r	$2V_{\text{avg}}R/\mathcal{D}$, radial Peclet number
Pe_z	axial Peclet number
r	radial coordinate (cm)
R	radius of the airway branch (cm)
Re	Reynolds number of the flowing gas
$\mathcal{R}_p$	mass transfer resistance of the capillary bed (s/cm)
Sc	Schmidt number
Sh	local Sherwood number
$\overline{\text{Sh}}$	average Sherwood number
$t_{1/2}$	$0.693/\kappa_t$, half-life of NO in pulmonary tissue (s)
V_z	axial gas velocity (cm/s)
V_{avg}	average axial gas velocity (cm/s)
x	r/R, dimensionless radial coordinate
y	coordinate for thickness of tissue and mucous layers (cm)
z	axial coordinate (cm)
α	dimensionless film coefficient
γ_n	eigenvalue
ξ	$(z/R\,\text{Pe}_r)$, dimensionless axial coordinate
κ	first order reaction rate constant (s^{-1})
λ	equilibrium partition coefficient
η_n	$\gamma_n x^2$
θ	$[C(r,z)-C_{\text{sat}}/C_0-C_{\text{sat}}]$, dimensionless gas phase concentration

SUBSCRIPTS

a	air (lumen)
b	capillary bed
$b{:}t$	at capillary bed:tissue boundary
m	mucous
$m{:}a$	at mucous:air boundary (i.e., wall of the airway lumen)
t	tissue
$t{:}m$	at tissue:mucous boundary
w	at wall of the airway lumen

REFERENCES

[1] Beckman, J. S., and W. H. Koppenol. Nitric oxide, superoxide, and peroxynitrite: The good, the bad, and the ugly. *J. Appl. Physiol.* 271:C1424–C1437, 1996.

[2] Bird, R. B., W. E. Stewart, and E. N. Lightfoot. Transport Phenomena. New York: Wiley, 1960, pp. 47, 140–146, 297, 366–370, 503–516, 601–619, 636–649.

[3] Bui, T. D., D. Dabdub, and S. C. George. Modeling the bronchial circulation with application to soluble gas exchange: Description and sensitivity analysis. *J. Appl. Physiol.* 84(6):2070–2088, 1998.

[4] Eckert, E. R. G., and R. M. Drake. Heat and Mass Transfer. New York: McGraw–Hill, 1959, pp. 131–153, 167–178.

[5] Fogler, H. S. Elements of Chemical Reaction Engineering, Prentice–Hall International Series, Englewood Cliffs, NJ: Prentice–Hall, 1992, pp. 731–733, 765–776.

[6] Gastineau, R. M., P. J. Walsh, and N. Underwood. Thickness

of bronchial epithelium with relation to exposure to radon. *Health Phys.* 23:860–861, 1972.
[7] Gaston, B., J. M. Drazen, J. Loscalzo, and J. S. Stamler. The biology of nitrogen oxides in the airways. *Am. J. Respir. Crit. Care Med.* 149:538–551, 1994.
[8] George, S. C., A. L. Babb, and M. P. Hlastala. Dynamics of soluble gas exchange in the airways III. Single-exhalation breathing maneuver. *J. Appl. Physiol.* 75:2439–2449, 1993.
[9] George, S. C., A. L. Babb, and M. P. Hlastala. Modeling the concentration of ethanol in exhaled breath following pretest breathing maneuvers. *Ann. Biomed. Eng.* 23:48–60, 1995.
[10] George, S. C., J. E. Souders, A. L. Babb, and M. P. Hlastala. Modeling steady-state inert gas exchange in the canine trachea. *J. Appl. Physiol.* 79:929–940, 1995.
[11] Grotberg, J. B. Gas absorption in pulmonary airways at low Peclet number. *J. Biomech. Eng.* 112:177–182, 1990.
[12] Hanna, L. M., and P. W. Scherer. Measurement of local mass transfer coefficients in a cast of the human upper respiratory tract. *J. Biomech. Eng.* 108:12–18, 1986.
[13] Hanna, L. M., and P. W. Scherer. A theoretical model of localized heat and water vapor transport in the human respiratory tract. *J. Biomech. Eng.* 108:19–27, 1986.
[14] Ingenito, E. P., J. Solway, E. R. McFadden, and J. M. Drazen. A quantitative study of heat transfer coefficients in the upper tracheobronchial tree of man (Abstract). *Fed. Proc.* 45:1020, 1986.
[15] International Critical Tables. New York: McGraw–Hill, 1928, Vol. 3, pp. 255–260.
[16] Jansen, A., J. Drazen, J. A. Osborne, R. Brown, J. Loscalzo, and J. S. Stamler. The relaxant properties in guinea pig airways of S-nitrosothiols. *J. Pharmacol. Exp. Therapeutics* 261:154–160, 1992.
[17] Kharitonov, V. G., A. R. Sundquist, and V. S. Sharma. Kinetics of nitrosation of thiols by nitric oxide in the presence of oxygen. *J. Biol. Chem.* 270:28158–28164, 1995.
[18] King, C. J. Separation Processes. New York: McGraw–Hill, 1980, pp. 524–527.
[19] Knudsen, J. G., and D. L. Katz. Fluid Dynamics and Heat Transfer. New York: McGraw–Hill, 1958.
[20] Lancaster, J. R. Simulation of the diffusion and reaction of endogenously produced nitric oxide. *Proc. Natl. Acad. Sci. USA* 91:8137–8141, 1994.
[21] Lancaster, J. R. Diffusion of free nitric oxide. *Methods Enzymol.* 268:31–49, 1996.
[22] Scherer, P. W., L. H. Shendalman, N. M. Greene, and A. Bouhuys. Measurement of axial diffusivities in a model of the bronchial airways. *J. Appl. Physiol.* 38:719–723, 1975.
[23] Souders, J. E., S. C. George, N. L. Polissar, E. R. Swenson, and M. P. Hlastala. Tracheal gas exchange: Perfusion-related differences in inert gas elimination. *J. Appl. Physiol.* 79:918–928, 1995.
[24] Ultman, J. S., and H. S. Blatman. Longitudinal mixing in pulmonary airways. Analysis of inert gas dispersion in symmetric tube network models. *Respir. Physiol.* 30:349–367, 1977.
[25] Weibel, E. Morphometry of the Human Lung. New York: Springer, 1963.
[26] Wink, D. A., M. B. Grisham, J. B. Mitchell, and P. C. Ford. Direct and indirect effects of nitric oxide in chemical reactions relevant to biology. *Methods Enzymol.* 268:12–31, 1996.
[27] Wink, D. A., R. W. Nims, J. F. Darbyshire, D. Christodoulou, I. Hanbauer, G. W. Cox, F. Laval, J. Laval, J. A. Cook, M. C. Krishna, W. G. DeGraff, and J. B. Mitchell. Reaction kinetics for nitrosation of cysteine and glutathione in aerobic nitric oxide solutions at neutral pH. Insights into the fate and physiological effects of intermediates generated in the NO/O_2 reaction. *Chem. Res. Toxicol.* 7:519–525, 1994.
[28] Wood, J., and J. Garthwaite. Models of the diffusional spread of nitric oxide: Implications for neutral nitric oxide signaling and its pharmacological properties. *Neuropharmacology* 33:1235–1244, 1994.
[29] Yung, C.-N., K. J. DeWitt, and T. G. Keith, Jr.. Three-dimensional steady flow through a bifurcation. *J. Biomech. Eng.* 112:189–197, 1990.